

Robust Attentive Deep Neural Network for Exposing GAN-generated Faces

Hui Guo, Shu Hu, Xin Wang, *Senior Member, IEEE*,
Ming-Ching Chang*, *Senior Member, IEEE* and Siwei Lyu, *Senior Member, IEEE*

Abstract—GAN-based techniques that generate and synthesize realistic faces have caused severe social concerns and security problems. Existing methods for detecting GAN-generated faces can perform well on limited public datasets. However, images from existing public datasets do not represent real-world scenarios well enough in terms of view variations and data distributions (where real faces largely outnumber synthetic faces). The state-of-the-art methods do not generalize well in real-world problems and lack the interpretability of detection results. Performance of existing GAN-face detection models degrades significantly when facing imbalanced data distributions. To address these shortcomings, we propose a robust, attentive, end-to-end network that can spot GAN-generated faces by analyzing their eye inconsistencies. Specifically, our model learns to identify inconsistent eye components by localizing and comparing the iris artifacts between the two eyes automatically. Our deep network addresses the imbalance learning issues by considering the AUC loss and the traditional cross-entropy loss jointly. Comprehensive evaluations of the FFHQ dataset in terms of both balanced and imbalanced scenarios demonstrate the superiority of the proposed method.

Index Terms—GAN-generated faces, face synthesis, Iris detection, attention models, ROC, AUC maximization.

I. INTRODUCTION

The development of Generative Adversarial Networks (GANs) [2] has led to a dramatic increase in the realism in generating high-quality face images, including StyleGAN [1] and PGGAN [3]. As illustrated in Figure 1, these GAN-generated fake faces are difficult to distinguish from human eyes. Such synthesized fake faces are easily generatable, can be directly leveraged for disinformation, and can potentially lead to profound social, security, and ethical impacts.

The GAN-generated faces can be easily abused for malicious purposes, such as creating fake social media accounts to lure or deceive unaware users [4]–[7], which can cause significant social security problems. Therefore, the authenticity of GAN-generated faces is increasingly valued recently, and there is a paucity of forensic techniques for specifically detecting such fake faces. Many studies employ CNNs or other classifiers to distinguish the GAN-generated faces from the real ones [8], [9]. Although these methods detect various GAN-generated faces with relatively high accuracy, they suffer, like other deep learning-based techniques, from lacking the interpretability of the detection results and poor generalization.

Hui Guo and Ming-Ching Chang are with University at Albany, SUNY, USA. (e-mail: hguo@albany.edu, mchang2@albany.edu)

Shu Hu and Siwei Lyu are with University at Buffalo, SUNY, USA. (e-mail: shuhu@buffalo.edu, siweilyu@buffalo.edu)

Xin Wang is with Keya Medical, USA. (e-mail: xinw@keyamedna.com)

*Corresponding author.



Fig. 1: Examples of GAN-generated (StyleGAN2 [1]) faces.

To resolve the above limitations, an explainable physical method was proposed in [10], they found inconsistencies between the corneal specular highlights of the two eyes in GAN-generated faces. Thus, the corneal specular highlights from two eyes are extracted and aligned for similarity comparison. However, their method has several limitations. When the portrait settings (For example, the two eyes have a frontal pose, both of eyes are far away from the light or reflection source, and all light sources are visible to both eyes) are disobeyed, false positives may raise, and it can not apply to face images where specular patterns are not present. In addition, their final detection results are from a rule-based method, which leads to a poor generalization problem.

Furthermore, all the existing works ignored the data imbalance problem, as in the real world, real images usually significantly outnumber GAN-generated images. As a result, it leads to an imbalanced data learning problem. In this situation, most of the existing classification losses such as cross entropy [11] are not suitable for classification with imbalanced data. Although existing sampling, adjust class weight and data enhancement have shown great success [12], [13], learning with the imbalanced dataset is still a challenging problem. Many studies have suggested that compared to simple classification losses, AUC (area under the receiver operating characteristic curve) is a robust evaluation measure for classification problem [14]. However, it is a pairwise rank-based metric and non-

differentiable. Therefore, directly minimize the AUC loss to train a classifier is usually impractical.

To resolve these issues, in this work, we propose a new unified deep learning framework for GAN-generated faces detection. Concretely, we first use Mask R-CNN [15] to detect the iris area. Then, motivated by [10], instead of corneal specular highlights segmentation, we use residual attention model [16] to localize the inconsistent components (such as corneal specular highlights) between the left and right iris and other artifacts automatically during the learning procedure. Finally, although AUC is non-differentiable and not easy to compute, several works [17], [18] had demonstrated that maximizing the alternative Wilcoxon-Mann-Whitney (WMW) statistic is equivalent to directly optimizing AUC. Inspired by [17], we jointly use an approximated AUC loss and Binary Cross Entropy (BCE) loss to optimize our framework. Experiment results based on the real human face images from the Flickr-Faces-HQ (FFHQ) dataset [1] and the GAN synthesized face images from <http://thispersondoesnotexist.com> demonstrate the superiority of our proposed framework on the GAN-generated faces detection task.

The main contributions of this paper are as follows:

- We proposed a unified framework, which uses an attention model to localize inconsistent components between the left and right iris and other artifacts automatically and provides interpretability of the results.
- Instead of sampling or data augmentation, we alleviate the impact of an imbalanced dataset by introducing an approximated AUC loss to optimize the AUC metric directly. This approach effectively addresses the imbalanced learning problem.
- By sampling the FFHQ datasets, we generate subsets to simulate real-world imbalanced data conditions and show that our method also achieved promising performance on the imbalanced datasets.

The paper is organized as follows. Section II summarizes the related work on GAN-generated faces detection, attention methods, and imbalanced learning. Section III introduces the proposed network architecture and the loss function for robust learning. In Section IV, we present and visualize the experimental results on the balanced and imbalanced datasets. Finally, we conclude this paper in Section V.

II. RELATED WORK

In this section, we briefly review related works that inspired this work, including GAN-generated faces detection methods and attention models. We also review the literature on the imbalanced learning problem.

A. GAN-generated faces detection

The GAN-generated faces detection methods can be divided into two categories.

Those in the first category are data-driven [19]–[23], where a deep neural network model is trained to identify real and GAN-generated faces. These deep learning (DL) based methods work well in some scenarios because they can learn more

information between image pixels in the high-dimensional feature space using neural networks.

Methods of the second category look for the explainable methods such as signal traces or artifacts left by the GAN synthesis model and physical/physiological inconsistencies by GAN methods. In papers [24], [25], the authors use the color difference to classify real images and GAN images. With the development of the GAN methods, the color difference can be fixed. More complicated methods, *e.g.*, [9], [26], use fingerprints or abstract signal-level traces in the noise residuals to differentiate GAN-generated faces. Since GAN generation leaves specific artifacts when doing the upsampling process, many works [27]–[29] recognize fake images based on these artifacts. In [30], the authors analyze the distributions of facial landmarks to distinguish GAN-generated faces, and [31] detects inconsistent head poses to expose the fake videos. Furthermore, [32] identifies GAN-generated faces by inspecting more visual aspects. The most recent work [10] uses the inconsistent corneal specular highlights between left and right eyes to expose GAN-generated faces. They show the proposed method efficiently on the frontal face images. However, as we discussed before, their method is limited to portrait settings.

B. Attention model

The research community pays attention to mechanisms to increase the interpretability of the deep learning model. For example, class activation mapping (CAM) [33] and Grad-CAM [34] are widely used in many computer vision tasks [35], [36]. However, they are only used to visually show significant parts in the images of the model prediction. Instead, integrating attention mechanisms into the neural network has been shown to be an effective strategy to boost performance, as the network is guided by attention to focus on important regions during training.

The channel attention is to focus on the relationship between channels to learn the importance of different channel information automatically. For example, SENet [36] embeds the channel attention mechanism into the residual block and proves the effectiveness of the channel attention mechanism on the large-scale image classification task. Moreover, to improve the representing ability of the network, [37] distinguishes the importance of the channels by attention mechanism.

Another line of attention model combines channel attention and spatial attention jointly [38], [39], to achieve a significant performance improvement. Residual Attention Network [16] combines a residual unit [40] with the attention mechanism by stacking residual attention block, which improves the network performance and reduces the complexity of the model better accuracy than ResNet [40].

C. Imbalanced learning

Imbalanced learning has been widely researched in machine learning [41], [42] and computer vision areas [43], [44]. In the early period, conventional solutions for the imbalanced learning methods are mainly based on sampling methods, such as oversampling, undersampling, and weighed sampling, etc [45]. For example, oversampling for the minor classes and

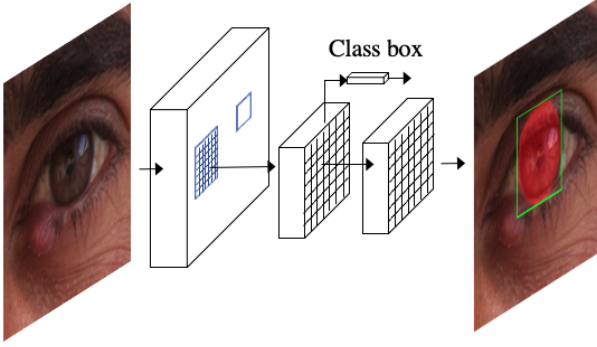


Fig. 2: Mask R-CNN for Iris Detection. The input is the cropped eye region image, and the outputs are the bounding box and its corresponding mask.

undersampling for the majority classes. However, the sampling methods have the following limitations. First of all, the undersampling may remove important and informative samples in the majority of classes. Furthermore, the oversampling could lead to an overfitting problem due to oversampled instances in the minor classes.

Another direction is the data augmentation-based methods, such as mirroring, rotation, etc., to expand data samples [46]. But, the main limitation of data augmentation is that the size of the original dataset still limits the diversity of the new augmented data samples.

III. METHOD

A. Overview

In this section, we present our approach for the GAN-generated faces detection framework. As is illustrated in Figure 4, our model first uses Mask R-CNN [15] to detect the left and right iris regions, and then it uses a residual attention based network [16] to perform binary estimation on the detected iris of left and right eyes, yielding the predicted result of real or GAN-generated. Finally, we present a detailed description of our joint loss function to address the data imbalance problem.

B. Iris Detection

As is mentioned in Sec. I, visible artifacts and inconsistencies can still be observed in the iris regions of GAN-generated images. Therefore, we employ an instance segmentation network to detect and segment the iris part for further investigation. The current state-of-the-art image instance segmentation system is Mask R-CNN [15]. The Mask R-CNN is based on Faster R-CNN [47], but adds a parallel branch for predicting object masks, it consists of two stages, as shown in Figure 2. The first stage is the Region Proposal Network (RPN). It generates candidate object bounding boxes for all the object categories. Then the second stage is the R-CNN stage, which extracts features using the Region of Interest Align (RoIAlign) layer for each proposal and performs classification, bounding box regression, and mask prediction.

In practice, we consider each iris as an instance to detect and segment. Concretely, the Mask R-CNN is trained using the eye region images from the datasets in [48], [49], more details

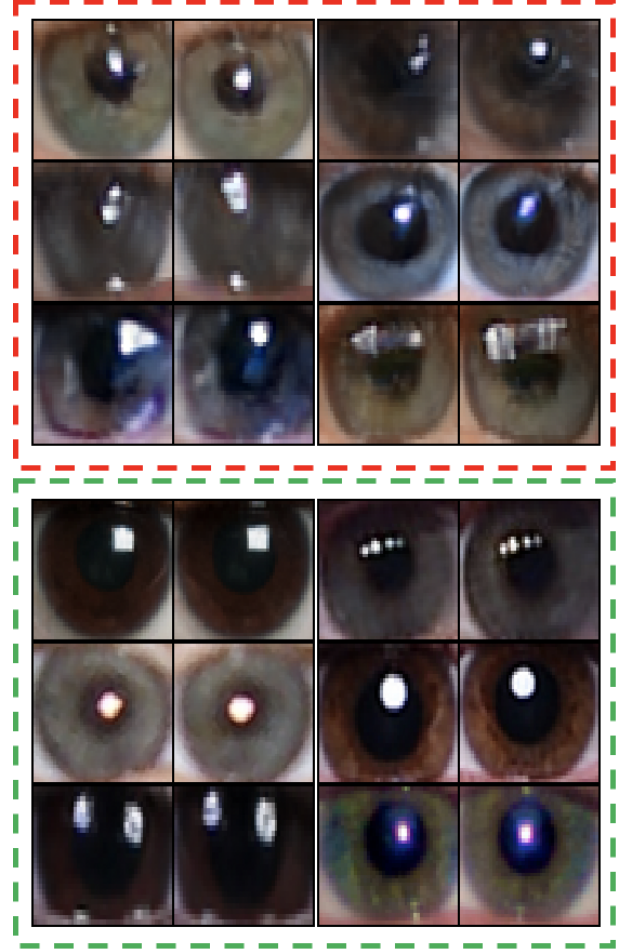


Fig. 3: Examples of iris pairs from the GAN-generated faces (Red box) and real faces (Green box). We can visually find that comparing with the real iris pairs, the GAN-generated iris pairs have inconsistent corneal specular highlights.

are described in Section IV-A2. During inference, given an input face image, we first use the face detector and landmark extractor provided in DLib [50] to the cropped eye region. We are then using the trained Mask R-CNN model to detect the iris and its mask. The iris examples for the real faces and GAN-generated faces are shown in Figure 3.

C. Network architectures

Inspired by the practices of the work [10], we use the attention mechanism in the network structure to develop an explainable and interpretable classification model. This is commonly accomplished by having a separate branch that calculates attention and is later incorporated back into the main branch with by weighing function. As is illustrated in Figure 5, our network architectures are mainly composed of residual attention blocks [16]. In each residual attention block, we have a trunk branch and a soft mask branch. The trunk branch performs feature processing, where we use residual unit [40]. And the soft mask branch uses a U-net structure [51] to weight output features.

Formally, given the input feature map f , the trunk branch T generates output $T(f)$ and the soft mask branch M generates

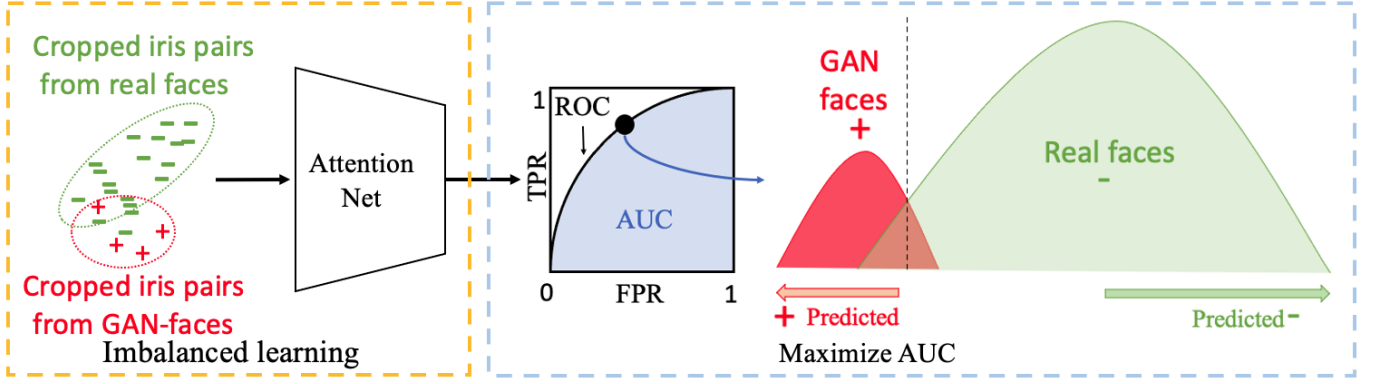


Fig. 4: The training processing of imbalanced learning. The extracted iris pairs are passed to the residual attention network for real or fake faces classification. Then, to alleviate the imbalanced learning problem, the classification network is optimized by the proposed robust loss function (see Section III-F for details) to maximize the AUC score.

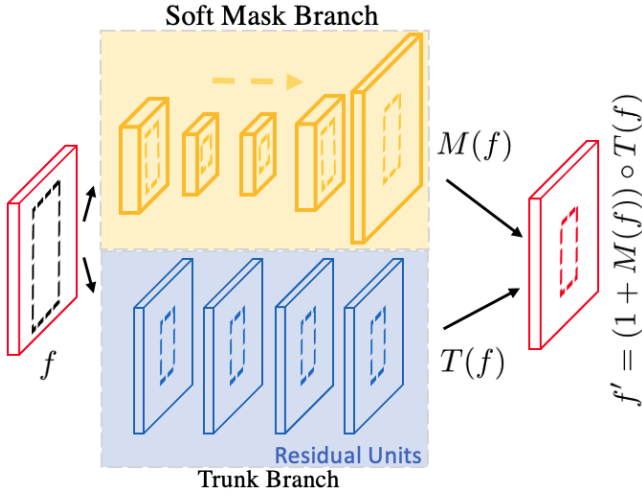


Fig. 5: Structures of the Attention Block.

soft mask map $M(f)$. The trunk branch contains only several residual blocks and acts as a shortcut for data flow. Afterward, the attention mask $M(f)$ is applied to the trunk branch to generate the attended feature map f' as $f' = (1 + M(f)) \circ T(f)$, where \circ denotes Hadamard product.

The attention module could be channel attention, spatial and mixed attention. As suggested in [16], the mixed attention has the best performance. Thus, we choose the mixed attention, which uses a sigmoid function $\frac{1}{1+\exp(-f_{s,c})}$ for each channel and each spatial location, where s ranges over all spatial positions and c ranges over all channels of f .

Finally, the overall real and fake iris classification network is constructed by stacking multiple residual attention blocks [16]. Although the attention module plays an important role in classification, a simple stacking of attention modules may reduce performance. A simple solution is adding the attention map onto the original feature map. This combination allows attention modules stacked like a ResNet [40] and improves the performance [16]. We summarize the details of the architectures in Table I. Given an input image, the network outputs its prediction score from the last Sigmoid function.

TABLE I: Details of the Network Architectures.

Layer	Output Size	Network
Conv1	$96 \times 96 \times 16$	3×3 , stride 1
Max pooling	$48 \times 48 \times 16$	3×3 , stride 2
Residual Unit	$48 \times 48 \times 64$	$1 \times \begin{bmatrix} 1 \times 1, 16 \\ 3 \times 3, 16 \\ 1 \times 1, 64 \\ 1 \times 1, 64 \end{bmatrix}$
Attention Block	$48 \times 48 \times 64$	attention $\times 2$
Residual Unit	$24 \times 24 \times 128$	$1 \times \begin{bmatrix} 1 \times 1, 32 \\ 3 \times 3, 32 \\ 1 \times 1, 128 \\ 1 \times 1, 128 \end{bmatrix}$
Attention Block	$24 \times 24 \times 128$	attention $\times 2$
Residual Unit	$12 \times 12 \times 256$	$1 \times \begin{bmatrix} 1 \times 1, 64 \\ 3 \times 3, 64 \\ 1 \times 1, 256 \\ 1 \times 1, 256 \end{bmatrix}$
Attention Block	$12 \times 12 \times 256$	attention $\times 2$
Residual Unit	$6 \times 6 \times 512$	$3 \times \begin{bmatrix} 1 \times 1, 128 \\ 3 \times 3, 128 \\ 1 \times 1, 512 \\ 1 \times 1, 512 \end{bmatrix}$
Average pooling	$1 \times 1 \times 512$	6×6 , stride 1
FC, Sigmoid	1	

D. AUC

Most of the existing classification loss functions, such as cross-entropy, are insufficient for addressing the data imbalance problem and cause the trained classification model to produce accurate but biased predictions, which may not fit the requirements of practical applications. It is desirable to use a specifically designed loss function to address data imbalances directly. Since the area under a receiver operation curve (AUC) [18], [52] is a robust evaluation metric for both balanced and imbalanced data, we would like to directly maximize the AUC to handle imbalanced situations.

AUC is widely used in the binary classification problems. We first review the definition of AUC. Suppose we have a set of data $\{(\mathbf{x}_i, y_i)\}_{i=1}^M$, where $\mathbf{x}_i \in \mathbb{R}^d$ and $y_i \in \{-1, +1\}$. We define a set of indices of positive instances as $\mathcal{P} = \{i | y_i = +1\}$. Similarly, we define the set of indices of negative instances as $\mathcal{N} = \{i | y_i = -1\}$. Then we have $M = |\mathcal{P}| + |\mathcal{N}|$. Denote $\mathbb{I}_{[a]}$ as an indicator function with $\mathbb{I}_{[a]} = 1$ if a is true and 0 otherwise. A binary classifier $c_{w,\lambda} : \mathbb{R}^d \rightarrow \{-1, +1\}$, is

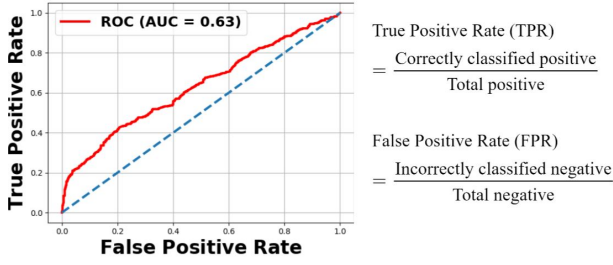


Fig. 6: An illustrative example of ROC and AUC.

defined as

$$c_{\mathbf{w},\lambda}(\mathbf{x}) = \text{sign}(g_{\mathbf{w}}(\mathbf{x}) - \lambda),$$

where $g_{\mathbf{w}} : \mathbb{R}^d \rightarrow \mathbb{R}$ is the parametric prediction function with parameter $\mathbf{w} \in \mathbb{R}^m$ and λ is the classification threshold. Denote $g_{\mathbf{w}}(\mathbf{x}_i)$ as the prediction score of the i -th sample, where $i \in \{1, \dots, M\}$. For simplicity, we assume $g_{\mathbf{w}}(\mathbf{x}_i) \neq g_{\mathbf{w}}(\mathbf{x}_j)$ for $i \neq j$ (ties can be broken in any consistent way).

Given a threshold λ , the number of negative examples with prediction scores larger than λ is called false positive (FP), and the number of positive examples with prediction scores greater or equal to λ is called true positive (TP). According to the FP and TP, we can define the false positive rate (FPR) and the true positive rate (TPR) as follows,

$$\text{FPR} = \frac{\sum_{i \in \mathcal{N}} \mathbb{I}[g_{\mathbf{w}}(\mathbf{x}_i) > \lambda]}{|\mathcal{N}|}, \quad \text{TPR} = \frac{\sum_{i \in \mathcal{P}} \mathbb{I}[g_{\mathbf{w}}(\mathbf{x}_i) \geq \lambda]}{|\mathcal{P}|}.$$

The receiver operation curve (ROC) is composed of FPR and TPR with setting different decision thresholds $\lambda \in (-\infty, \infty)$. Based on this definition, ROC is a curve confined to $[0, 1] \times [0, 1]$ and connecting the point (0,0) to the point (1,1). Then AUC corresponds to the area enclosed by the ROC. Figure 6 provides an illustrative example of ROC and AUC. We can find that the more bowed the ROC curve is toward the upper left corner, the higher the AUC score, which means the better the classifier's ability to discriminate between the two classes.

E. AUC Relaxation

The computation of an AUC score based on the area under a ROC curve cannot be directly used in a loss function. However, according to the Wilcoxon-Mann-Whitney (WMW) statistic [17], we can relax AUC as follows,

$$\text{AUC} = \frac{1}{|\mathcal{P}||\mathcal{N}|} \sum_{i \in \mathcal{P}} \sum_{j \in \mathcal{N}} \mathbb{I}[g_{\mathbf{w}}(\mathbf{x}_i) > g_{\mathbf{w}}(\mathbf{x}_j)].$$

Therefore, the corresponding AUC loss (risk) can be defined as

$$\mathcal{L}_{\text{AUC}} = 1 - \text{AUC} = \frac{1}{|\mathcal{P}||\mathcal{N}|} \sum_{i \in \mathcal{P}} \sum_{j \in \mathcal{N}} \mathbb{I}[g_{\mathbf{w}}(\mathbf{x}_i) < g_{\mathbf{w}}(\mathbf{x}_j)]. \quad (1)$$

Obviously, \mathcal{L}_{AUC} takes value in $[0, 1]$. It is a fraction of pairs of prediction scores from the positive sample and negative sample that are ranked incorrectly, i.e., the prediction score from a negative sample is larger than the prediction score from a positive sample. If all prediction scores from the positive samples are larger than any prediction score from the negative samples, then $\mathcal{L}_{\text{AUC}} = 0$. This indicates we obtain a perfect

classifier. Furthermore, \mathcal{L}_{AUC} is independent of the threshold λ . It only depends on the prediction scores $g_{\mathbf{w}}(\mathbf{x})$. In other words, the predictor $g_{\mathbf{w}}$ affects the value of \mathcal{L}_{AUC} . Therefore, we aim to learn a classifier $g_{\mathbf{w}}$ that minimizes Eq.(1).

Although we can calculate \mathcal{L}_{AUC} by comparing prediction score from the positive sample and prediction score from the negative sample in each pair, the \mathcal{L}_{AUC} formulation is non-differentiable due to the discrete computation. It is therefore desirable to find a differentiable approximation for \mathcal{L}_{AUC} . Inspired by the work in [17], we find an approximation to \mathcal{L}_{AUC} that can be directly applied to our objective function to minimize the AUC loss along with our imbalanced training procedure. Specifically, a differentiable approximation of \mathcal{L}_{AUC} can be formulated as:

$$\mathcal{L}_{\text{AUC}} = \frac{1}{|\mathcal{P}||\mathcal{N}|} \sum_{i \in \mathcal{P}} \sum_{j \in \mathcal{N}} R(g_{\mathbf{w}}(\mathbf{x}_i), g_{\mathbf{w}}(\mathbf{x}_j)), \quad (2)$$

where

$$R(g_{\mathbf{w}}(\mathbf{x}_i), g_{\mathbf{w}}(\mathbf{x}_j)) = \begin{cases} (-g_{\mathbf{w}}(\mathbf{x}_i) - g_{\mathbf{w}}(\mathbf{x}_j) - \gamma)^p, & g_{\mathbf{w}}(\mathbf{x}_i) - g_{\mathbf{w}}(\mathbf{x}_j) < \gamma, \\ 0, & \text{otherwise,} \end{cases} \quad (3)$$

$\gamma \in (0, 1]$ and $p > 1$ are two hyperparameters.

F. Loss Function

More specifically, we propose a joint loss function comprising the conventional binary cross-entropy (BCE) loss function \mathcal{L}_{BCE} and the AUC loss function \mathcal{L}_{AUC} (Eq.(2)). Therefore, the final loss function of our model becomes:

$$\mathcal{L} = \alpha \mathcal{L}_{\text{BCE}} + (1 - \alpha) \mathcal{L}_{\text{AUC}}, \quad (4)$$

where $\alpha \in [0, 1]$ is a scaling factor that is designed for balancing the weights of the BCE loss and the AUC loss.

IV. EXPERIMENT

In the following subsections, we first introduce the datasets and implementation details, then we compare the performance of our model with that of some advanced methods. We also evaluate the performance of our model on the imbalanced datasets. Finally, we perform a series of ablation experiments and show some qualitative results.

A. Experiment Setting

1) *Dataset*: The images of real human eyes are obtained from the Flickr-Faces-HQ (FFHQ) dataset [1], and the GAN-generated human faces are created by the StyleGAN2 method [1]. The images have a resolution of 1024×1024 pixels. We randomly select 5000 real face images from FFHQ and 5000 fake face images from <http://thispersondoesnotexist.com>. After iris detection, we have 3739 real iris pairs and 3748 fake iris pairs available as our final dataset. The training and testing spilled ratio is 8:2.

Furthermore, to evaluate the detection performance of our proposed framework and the compared methods when facing both balanced and imbalanced datasets in real applications. We mimic real-world situations wherein real face images significantly outnumber GAN-generated images, we sampled

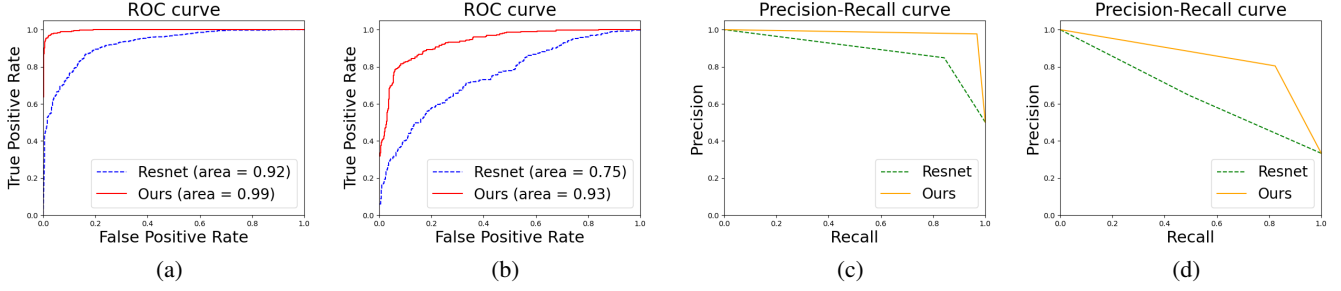


Fig. 7: Comparison of our model with BCE+AUC loss and Resnet with BCE loss. **Top:** (a) ROC on the balanced dataset FFHQ-b and (b) imbalanced dataset FFHQ-imb. **Bottom:** (c) Precision-Recall curve on the balanced dataset FFHQ-b and (d) imbalanced dataset FFHQ-imb.

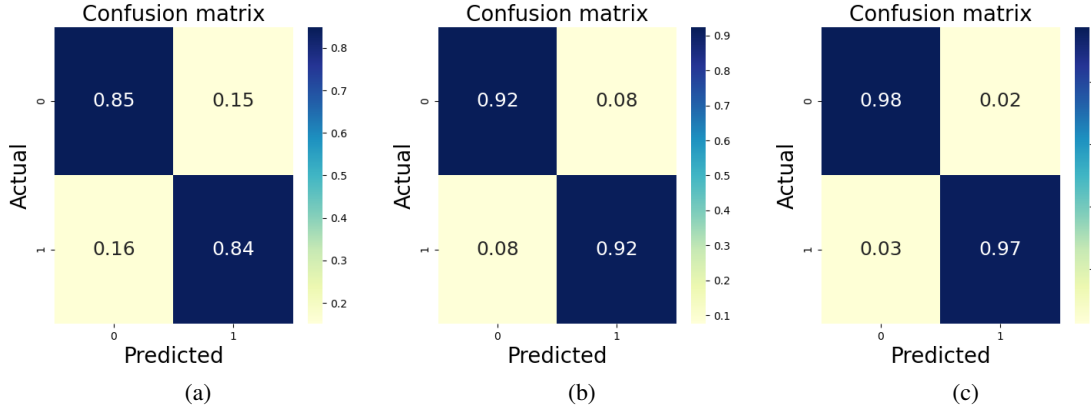


Fig. 8: Confusion Matrix on the balanced dataset FFHQ-b. (a) Resnet with BCE loss. (b) Our model with BCE loss. (c) Our model with BCE+AUC loss.

TABLE II: Details of the two types of datasets.

Datasets	Train		Test		Ratio \approx
	GAN-face	Real	GAN-face	Real	
FFHQ-b	2998	2991	750	748	1:1
FFHQ-imb	1200	2400	300	600	1:2

imbalanced subsets from our final dataset. Details of our datasets are described in Table II, where FFHQ-b indicates a balanced dataset, and FFHQ-imb indicates the imbalanced dataset with GAN-generated faces (positive) to real faces (negative) ratio of 1:2.

2) *Implementation Details:* The whole framework is implemented in Pytorch [53]. We conduct the experiments on two NVIDIA GeForce GPUs.

For the iris detection part, the Mask R-CNN is trained using the datasets in [48]. For each training eye image, the iris outer boundary mask is provided by [48] with default hyper-parameters settings, we use it to generate the bounding box and its corresponding mask for training purposes, and using the default training settings in [15]. In the testing stage, given an input face image, we first use the face detector and landmark extractor provided in DLib [50] to cropped eye regions. Then we pass the cropped eye regions to the trained Mask R-CNN model to predict the iris bounding boxes and their corresponding masks for both left and right eyes. Then we crop the left and right iris based on the bounding box and concatenate them as the input of our classification network. The image size of cropped iris is 128×128 , the size of the

concatenated image is 128×256 .

For the iris classification part, the overall network architecture is described in Table I. The network stacks of 3 stages residual attention models. The network is trained using Adam optimizer [54] with a learning rate of 0.001. We terminate training at 100 iterations. We resize the 128×256 concatenated images to 96×96 images for training and testing.

For the hyper-parameters, we set $p = 2$ (Eq. 3) and $\gamma = 0.4$ (Eq. 3) in all the experiments. For the experiments on the balanced dataset, the α (Eq. 4) is set to 0.2. For the experiments on the imbalanced dataset, the α is set to 0.4. These hyperparameters can provide us the best model performance.

3) *Evaluation Metrics:* In this study, we use Accuracy (ACC), Precision (P), Recall (R), F1 score (F1), the area under the ROC curve (AUC), and Precision-Recall (PR) curve as the evaluation metrics. Formally, the ACC is defined as $ACC = \frac{TP+TN}{TP+TN+FP+FN}$, where TP , FN , FP and TN indicate the true positives, false negatives, the false positives, and the true negatives, respectively. The Precision and recall are defined as $P = \frac{TP}{TP+FP}$ and $R = \frac{TP}{TP+FN}$. F1 score is the harmonic average value of P and R. It is defined as $F1 = \frac{2PR}{P+R}$. The PR curve shows the relationship between Precision and Recall.

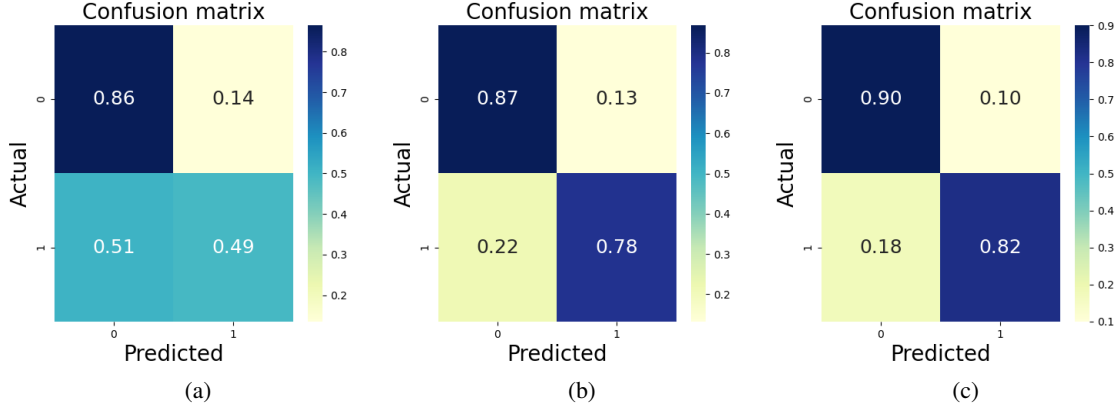


Fig. 9: Confusion Matrix on the imbalanced dataset FFHQ-imb. (a) Resnet with BCE loss. (b) Our model with BCE loss. (c) Our model with BCE+AUC loss.

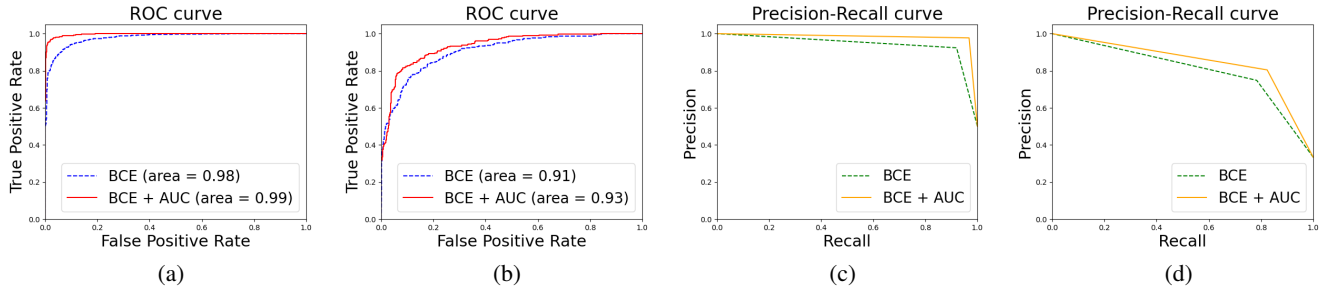


Fig. 10: Evaluation the effectiveness of the AUC loss function, comparison between our network with BCE loss and our network with BCE+AUC loss. **Top:** (a) ROC on the balanced dataset FFHQ-b and (b) imbalanced dataset FFHQ-imb. **Bottom:** (c) Precision-Recall curve on the balanced dataset FFHQ-b and (d) imbalanced dataset FFHQ-imb.

TABLE III: Robustness results on the the dataset FFHQ-b.

Method	Metric				
	ACC	P	R	F1	AUC
Resnet [40]	0.85	0.85	0.84	0.85	0.92
Ours	0.97	0.98	0.97	0.97	0.99

TABLE IV: Robustness results on the the dataset FFHQ-imb.

Method	Metric				
	ACC	P	R	F1	AUC
Resnet [40]	0.74	0.65	0.49	0.56	0.75
Ours	0.87	0.80	0.82	0.81	0.93

TABLE V: Ablation Study on the FFHQ-b dataset.

Loss	Metric				
	ACC	P	R	F1	AUC
BCE	0.92	0.92	0.92	0.92	0.98
BCE+AUC	0.97	0.98	0.97	0.97	0.99

TABLE VI: Ablation Study on the FFHQ-imb dataset.

Loss	Metric				
	ACC	P	R	F1	AUC
BCE	0.84	0.75	0.78	0.77	0.91
BCE+AUC	0.87	0.80	0.82	0.81	0.93

B. Evaluation on the balanced dataset

To evaluate the effectiveness of the proposed method, we evaluate the proposed framework against the most advanced classification model, ResNet [40]. We present the classification results of different methods on the balanced FFHQ dataset in Table III. We also show the ROC curve in Figure 7 (a) and the PR curve in Figure 7 (c). The corresponding Confusion matrix are shown in Figure 8 (a) and (c). It can be observed that our method achieves the highest performance compared with the compared method in all metrics. This indicates the superior ability of our method in the GAN-face detection task.

C. Evaluation on the imbalanced dataset

To verify the effectiveness of the proposed approach for the imbalanced learning problem, we also present the classification

results of different methods on the imbalanced datasets in Table IV. We also show the ROC curve in Figure 7 (b) and the PR curve in Figure 7 (d). The corresponding Confusion Matrix are shown in Figure 9 (a) and (c). These results indicate that our AUC loss boosts the performance for GAN-generated faces detection on both balanced and imbalanced datasets.

D. Ablation Study of AUC loss

In this section, we evaluate the effectiveness of the AUC loss function through an ablation study on both balanced and imbalanced datasets. Table V and VI show the experimental results of the ablation study. When only using the BCE loss, the AUC score for all the evaluation metrics decreased. The ROC and PR curves are also shown in Figure 10. The corresponding Confusion Matrix are shown in Figure 8 (b)

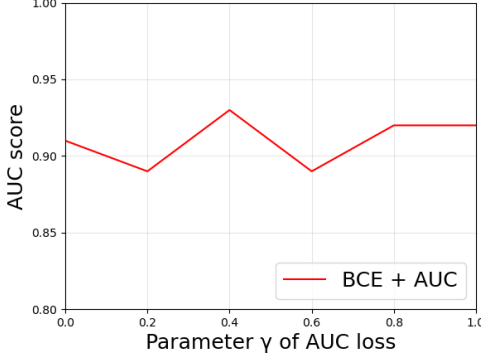


Fig. 11: Impact of hyperparameter γ in the AUC loss (Eq.(3)) for the GAN-generated faces detection on the imbalanced dataset.

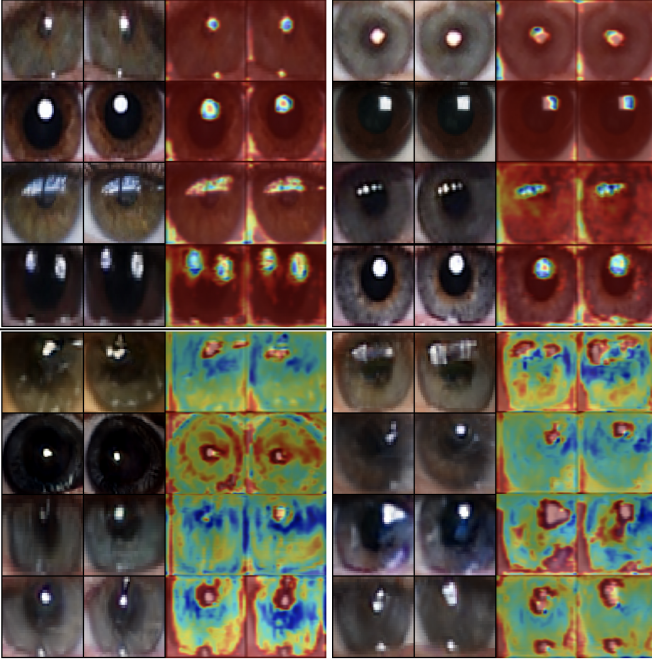


Fig. 12: Examples of iris and the corresponding attention maps. **Top 4 rows:** From real human faces. **Bottom 4 rows:** From GAN-generated human faces.

and Figure 9 (b). Experimental results show that our proposed method outperforms the ResNet at all evaluation metrics. This proves that the AUC loss can improve the classification consistently and substantially.

E. Hyper-parameter Analysis

We also study the impact of hyper-parameter γ in the AUC loss on the detection performance on the imbalanced dataset. The experimental results are shown in Figure. 11. We report the AUC score when γ changes from 0.0 to 1.0. The AUC score achieves the best for GAN-generated faces detection when $\gamma = 0.4$.

F. Qualitative Results

In Figure 12, we provide visualization of the attention maps of the real and GAN-generated iris examples. It can be observed that there is an obvious difference between the corresponding attention maps of fake iris (GAN-generated) and real samples. Concretely, the network attends on the whole iris part for the real images and attends to the highlight parts for the fake images.

V. CONCLUSION

In this work, we investigate building a robust deep learning-based framework for exposing GAN-synthesized faces. We first use Mask R-CNN to detect the iris area. Then, we use the residual attention model to localize the inconsistent components between the left and right iris and other artifacts automatically during the learning procedure. Finally, we also optimize the Wilcoxon-Mann-Whitney (WMW) statistic alternatively to directly maximizing the AUC score. Our model has shown appealing properties which overcome several shortcomings of existing GAN-generated faces detection methods. The experimental results show that our model achieves superior performance on both balanced and imbalanced datasets for the GAN-generated faces detection task.

REFERENCES

- [1] T. Karras, S. Laine, and T. Aila, “A style-based generator architecture for generative adversarial networks,” in *Proceedings of the IEEE/CVF Conference on Computer Vision and Pattern Recognition*, 2019, pp. 4401–4410.
- [2] I. J. Goodfellow, J. Pouget-Abadie, M. Mirza, B. Xu, D. Warde-Farley, S. Ozair, A. Courville, and Y. Bengio, “Generative adversarial networks,” *NIPS*, 2014.
- [3] T. Karras, T. Aila, S. Laine, and J. Lehtinen, “Progressive growing of gans for improved quality, stability, and variation,” *arXiv preprint arXiv:1710.10196*, 2017.
- [4] “A spy reportedly used an ai-generated profile picture to connect with sources on linkedin,” <https://bit.ly/35BU215>.
- [5] “A high school student created a fake 2020 US candidate. twitter verified it,” <https://www.cnn.com/2020/02/28/tech/fake-twitter-candidate-2020/index.html>.
- [6] “How fake faces are being weaponized online,” <https://www.cnn.com/2020/02/20/tech/fake-faces-deepfake/index.html>.
- [7] “These faces are not real,” <https://graphics.reuters.com/CYBER-DEEPFAKE/ACTIVIST/nmovajgnxpa/index.html>.
- [8] X. Yang, Y. Li, and S. Lyu, “Exposing deep fakes using inconsistent head poses,” in *ICASSP 2019-2019 IEEE International Conference on Acoustics, Speech and Signal Processing (ICASSP)*. IEEE, 2019, pp. 8261–8265.
- [9] F. Marra, D. Gragnaniello, L. Verdoliva, and G. Poggi, “Do gans leave artificial fingerprints?” in *2019 IEEE Conference on Multimedia Information Processing and Retrieval (MIPR)*. IEEE, 2019, pp. 506–511.
- [10] S. Hu, Y. Li, and S. Lyu, “Exposing gan-generated faces using inconsistent corneal specular highlights,” in *ICASSP 2021-2021 IEEE International Conference on Acoustics, Speech and Signal Processing (ICASSP)*. IEEE, 2021, pp. 2500–2504.
- [11] K. P. Murphy, *Machine learning: a probabilistic perspective*. MIT press, 2012.
- [12] M. Fadaee, A. Bisazza, and C. Monz, “Data augmentation for low-resource neural machine translation,” *arXiv preprint arXiv:1705.00440*, 2017.
- [13] C. Szegedy, W. Liu, Y. Jia, P. Sermanet, S. Reed, D. Anguelov, D. Erhan, V. Vanhoucke, and A. Rabinovich, “Going deeper with convolutions,” in *CVPR*, 2015, pp. 1–9.
- [14] F. J. Provost, T. Fawcett, R. Kohavi *et al.*, “The case against accuracy estimation for comparing induction algorithms,” in *ICML*, vol. 98, 1998, pp. 445–453.

- [15] K. He, G. Gkioxari, P. Dollár, and R. Girshick, "Mask r-cnn," in *Proceedings of the IEEE international conference on computer vision*, 2017, pp. 2961–2969.
- [16] F. Wang, M. Jiang, C. Qian, S. Yang, C. Li, H. Zhang, X. Wang, and X. Tang, "Residual attention network for image classification," in *Proceedings of the IEEE conference on computer vision and pattern recognition*, 2017, pp. 3156–3164.
- [17] L. Yan, R. H. Dodier, M. Mozer, and R. H. Wolniewicz, "Optimizing classifier performance via an approximation to the wilcoxon-mann-whitney statistic," in *Proceedings of the 20th international conference on machine learning (ICML)*, 2003, pp. 848–855.
- [18] S. Lyu and Y. Ying, "A univariate bound of area under roc," in *Proceedings of the Conference on Uncertainty on Artificial Intelligence (UAI)*, 2018.
- [19] F. Marra, C. Saltori, G. Boato, and L. Verdoliva, "Incremental learning for the detection and classification of gan-generated images," in *2019 IEEE International Workshop on Information Forensics and Security (WIFS)*. IEEE, 2019, pp. 1–6.
- [20] M. Goebel, L. Nataraj, T. Nanjundaswamy, T. M. Mohammed, S. Chandrasekaran, and B. Manjunath, "Detection, attribution and localization of gan generated images," *arXiv preprint arXiv:2007.10466*, 2020.
- [21] S.-Y. Wang, O. Wang, R. Zhang, A. Owens, and A. A. Efros, "Cnn-generated images are surprisingly easy to spot... for now," in *Proceedings of the IEEE Conference on Computer Vision and Pattern Recognition*, vol. 7, 2020.
- [22] Z. Liu, X. Qi, and P. H. Torr, "Global texture enhancement for fake face detection in the wild," in *Proceedings of the IEEE/CVF Conference on Computer Vision and Pattern Recognition*, 2020, pp. 8060–8069.
- [23] N. Hulzebosch, S. Ibrahim, and M. Worring, "Detecting cnn-generated facial images in real-world scenarios," in *Proceedings of the IEEE/CVF Conference on Computer Vision and Pattern Recognition Workshops*, 2020, pp. 642–643.
- [24] S. McCloskey and M. Albright, "Detecting gan-generated imagery using color cues," *arXiv preprint arXiv:1812.08247*, 2018.
- [25] H. Li, B. Li, S. Tan, and J. Huang, "Detection of deep network generated images using disparities in color components," *arXiv preprint arXiv:1808.07276*, 2018.
- [26] N. Yu, L. S. Davis, and M. Fritz, "Attributing fake images to gans: Learning and analyzing gan fingerprints," in *Proceedings of the IEEE International Conference on Computer Vision*, 2019, pp. 7556–7566.
- [27] X. Zhang, S. Karaman, and S.-F. Chang, "Detecting and simulating artifacts in gan fake images," in *2019 IEEE International Workshop on Information Forensics and Security (WIFS)*. IEEE, 2019, pp. 1–6.
- [28] J. Frank, T. Eisenhofer, L. Schönherr, A. Fischer, D. Kolossa, and T. Holz, "Leveraging frequency analysis for deep fake image recognition," *arXiv preprint arXiv:2003.08685*, 2020.
- [29] R. Durall, M. Keuper, and J. Keuper, "Watch your up-convolution: Cnn based generative deep neural networks are failing to reproduce spectral distributions," in *Proceedings of the IEEE/CVF Conference on Computer Vision and Pattern Recognition*, 2020, pp. 7890–7899.
- [30] X. Yang, Y. Li, H. Qi, and S. Lyu, "Exposing gan-synthesized faces using landmark locations," in *ACM Workshop on Information Hiding and Multimedia Security (IHMMSec)*, 2019.
- [31] X. Yang, Y. Li, and S. Lyu, "Exposing deep fakes using inconsistent head poses," in *ICASSP*, 2019.
- [32] F. Matern, C. Riess, and M. Stamminger, "Exploiting visual artifacts to expose deepfakes and face manipulations," in *2019 IEEE Winter Applications of Computer Vision Workshops (WACVW)*. IEEE, 2019, pp. 83–92.
- [33] B. Zhou, A. Khosla, A. Lapedriza, A. Oliva, and A. Torralba, "Learning deep features for discriminative localization," in *Proceedings of the IEEE conference on computer vision and pattern recognition*, 2016, pp. 2921–2929.
- [34] R. R. Selvaraju, M. Cogswell, A. Das, R. Vedantam, D. Parikh, and D. Batra, "Grad-cam: Visual explanations from deep networks via gradient-based localization," in *Proceedings of the IEEE international conference on computer vision*, 2017, pp. 618–626.
- [35] A. Chattopadhyay, A. Sarkar, P. Howlader, and V. N. Balasubramanian, "Grad-cam++: Generalized gradient-based visual explanations for deep convolutional networks," in *2018 IEEE Winter Conference on Applications of Computer Vision (WACV)*. IEEE, 2018, pp. 839–847.
- [36] J. Hu, L. Shen, and G. Sun, "Squeeze-and-excitation networks," in *Proceedings of the IEEE conference on computer vision and pattern recognition*, 2018, pp. 7132–7141.
- [37] Y. Zhang, K. Li, K. Li, L. Wang, B. Zhong, and Y. Fu, "Image super-resolution using very deep residual channel attention networks," in *Proceedings of the European Conference on Computer Vision (ECCV)*, 2018, pp. 286–301.
- [38] L. Chen, H. Zhang, J. Xiao, L. Nie, J. Shao, W. Liu, and T.-S. Chua, "Sca-cnn: Spatial and channel-wise attention in convolutional networks for image captioning," in *Proceedings of the IEEE conference on computer vision and pattern recognition*, 2017, pp. 5659–5667.
- [39] S. Woo, J. Park, J.-Y. Lee, and I. So Kweon, "Cbam: Convolutional block attention module," in *Proceedings of the European conference on computer vision (ECCV)*, 2018, pp. 3–19.
- [40] K. He, X. Zhang, S. Ren, and J. Sun, "Deep residual learning for image recognition," in *Proceedings of the IEEE conference on computer vision and pattern recognition*, 2016, pp. 770–778.
- [41] Y. Yang and Z. Xu, "Rethinking the value of labels for improving class-imbalanced learning," *arXiv preprint arXiv:2006.07529*, 2020.
- [42] K. Cao, C. Wei, A. Gaidon, N. Aréchiga, and T. Ma, "Learning imbalanced datasets with label-distribution-aware margin loss," in *Proceedings of the 33rd International Conference on Neural Information Processing Systems*, 2019, pp. 1567–1578.
- [43] Y. Wang, W. Gan, J. Yang, W. Wu, and J. Yan, "Dynamic curriculum learning for imbalanced data classification," in *Proceedings of the IEEE/CVF International Conference on Computer Vision*, 2019, pp. 5017–5026.
- [44] C. Huang, Y. Li, C. C. Loy, and X. Tang, "Learning deep representation for imbalanced classification," in *Proceedings of the IEEE conference on computer vision and pattern recognition*, 2016, pp. 5375–5384.
- [45] H. He and E. A. Garcia, "Learning from imbalanced data," *IEEE Transactions on knowledge and data engineering*, vol. 21, no. 9, pp. 1263–1284, 2009.
- [46] C. Shorten and T. M. Khoshgoftaar, "A survey on image data augmentation for deep learning," *Journal of Big Data*, vol. 6, no. 1, pp. 1–48, 2019.
- [47] S. Ren, K. He, R. Girshick, and J. Sun, "Faster r-cnn: Towards real-time object detection with region proposal networks," *arXiv preprint arXiv:1506.01497*, 2015.
- [48] C. Wang, J. Muhammad, Y. Wang, Z. He, and Z. Sun, "Towards complete and accurate iris segmentation using deep multi-task attention network for non-cooperative iris recognition," *IEEE Transactions on Information Forensics and Security*, vol. 15, pp. 2944–2959, 2020.
- [49] C. Wang, Y. Wang, K. Zhang, J. Muhammad, T. Lu, Q. Zhang, Q. Tian, Z. He, Z. Sun, Y. Zhang *et al.*, "Nir iris challenge evaluation in non-cooperative environments: Segmentation and localization," in *2021 IEEE International Joint Conference on Biometrics (IJCB)*. IEEE, 2021, pp. 1–10.
- [50] D. E. King, "Dlib-ml: A machine learning toolkit," *Journal of Machine Learning Research*, vol. 10, pp. 1755–1758, 2009.
- [51] O. Ronneberger, P. Fischer, and T. Brox, "U-net: Convolutional networks for biomedical image segmentation," in *International Conference on Medical image computing and computer-assisted intervention*. Springer, 2015, pp. 234–241.
- [52] C. Cortes and M. Mohri, "Auc optimization vs. error rate minimization," *Advances in neural information processing systems*, vol. 16, pp. 313–320, 2003.
- [53] A. Paszke, S. Gross, F. Massa, A. Lerer, J. Bradbury, G. Chanan, T. Killeen, Z. Lin, N. Gimelshein, L. Antiga *et al.*, "Pytorch: An imperative style, high-performance deep learning library," *Advances in neural information processing systems*, vol. 32, pp. 8026–8037, 2019.
- [54] D. P. Kingma and J. Ba, "Adam: A method for stochastic optimization," in *ICLR (Poster)*, 2015.